

Journal of Materials Chemistry A

# **Transition Metal-Substituted Lead Halide Perovskite Absorbers**

Journal:	Journal of Materials Chemistry A
Manuscript ID	TA-ART-11-2016-009745.R2
Article Type:	Paper
Date Submitted by the Author:	03-Jan-2017
Complete List of Authors:	Sampson, Matthew; Argonne National Laboratory, Materials Science Division Park, Ji-Sang; Argonne National Laboratory, Center for Nanoscale Materials Schaller, Richard; Argonne National Laboratory, Center for Nanoscale Materials Chan, Maria; Argonne National Laboratory, Center for Nanoscale Materials Martinson, Alex; Argonne National Laboratory, Materials Science Division

SCHOLARONE™ Manuscripts



# Journal of Materials Chemistry A

## **Materials for Energy and Sustainability**

Full paper submission

Journal of Materials Chemistry A is a weekly journal in the materials field. The journal is interdisciplinary, publishing work of international significance on all aspects of materials chemistry related to energy and sustainability. Articles cover the fabrication, properties and applications of materials.

2015 Impact Factor of *Journal of Materials Chemistry A*: **8.262** For more information go to <a href="https://www.rsc.org/materialsA">www.rsc.org/materialsA</a>

The following paper has been submitted to *Journal of Materials Chemistry A* for consideration as a **Full paper**.

The Editorial Board stress a very high quality and novelty standard is needed for acceptance.

Journal of Materials Chemistry A wishes to publish original research that demonstrates significant **novelty** and advance, either in the chemistry used to produce materials or in the properties/applications of the materials produced. Work submitted that is outside of these criteria will not usually be considered for publication. The materials should also be related to the theme of materials for energy and sustainability.

We ask referees to examine manuscripts very carefully, and recommend rejection of articles which do not meet our high novelty, quality and impact expectations. Please note that **the rejection rate for JMCA is currently ~80%** of submitted manuscripts. **Routine or incremental** work, however competently researched and reported, should not be recommended for publication if it does not meet our expectations with regard to novelty and impact.

It is the responsibility of authors to provide fully convincing evidence for the homogeneity and identity of all compounds they claim as new. Evidence of both purity and identity is required to establish that the properties and constants reported are those of the compound with the new structure claimed.

Thank you for your effort in reviewing this submission. It is only through the continued service of referees that we can maintain both the high quality of the publication and the rapid response times to authors. We would greatly appreciate if you could review this paper in **ten days**. Please let us know if that will not be possible.

Once again, we appreciate your time in serving as a reviewer. To acknowledge this, the Royal Society of Chemistry offers a **25% discount** on its books: <a href="http://www.rsc.org/Shop/books/discounts.asp">http://www.rsc.org/Shop/books/discounts.asp</a>. Please also consider submitting your next manuscript to *Journal of Materials Chemistry A*.

Best wishes,

Dr Fiona McKenzie

FMCCONZLE

Executive Editor, Journal of Materials Chemistry A



January 3, 2017

Prof. Michael Chabinyc Associate Editor, *J. Mater. Chem. A* Materials Department University of California, Santa Barbara

Dear Prof. Chabinyc,

Thank you for handling our manuscript titled "Transition Metal-Substituted Lead Halide Perovskite Absorbers". We thank you for your careful consideration of the manuscript and for the opportunity to address the referees' revision requests. Per your instructions we have addressed the reviewer suggestion. Please find our point-by-point response in-line below.

I trust that with these revisions the manuscript can be accepted for publication in the *Journal of Materials Chemistry A*.

Thank you for your consideration,

Alex Martinson

Alex Wenter

Chemist

#### **Materials Science Division**

Argonne National Laboratory 9700 South Cass Avenue, Bldg. 241 Argonne, IL 60439

1-630-252-7520 phone 1-630-252-9555 fax martinson@anl.gov Referee: 1

#### Comments to the Author:

The authors have sufficiently addressed the issues previously reported. One very minor suggestion, in response to the comment: "The authors should note that there is a previous report in the literature of an Hg-doped intermediate band PV based off of MAPbBr3 (DOI: 10.1007/s11082-016-0525-y) and compare and contrast with their results." The authors have included the reference, and in the response they provide a nice discussion comparing and contrasting this work with theirs. I think it would be a nice point to address in the manuscript, showing why the authors' work differs from and improves upon this report.

We thank the referee for this minor suggestion, and we have added the text from our previous response to the Results and Discussion section of the manuscript (pg. 6-7). Specifically, we added:

"These experimental and computational findings improve upon the work of Andalibi et al., which reports the computed electronic structure of Hg-doped MAPbI<sub>3</sub> (band gap =  $1.5 \sim 1.6$  eV). We note that this study differs in the perovskite system under investigation and reports only on a computational modeling by DFT. Our study differs substantially in its investigation of substituting 3d transition metals with open shells in MAPbBr<sub>3</sub>. The Hg-induced IB has no s or p orbital character, indicating that it has mainly d and/or f orbital characters. The full d shell of Hg is more likely to be filled and therefore not as effective as an IB, compared to those introduced by the 3d dopants in the current study."

# ROYAL SOCIETY OF CHEMISTRY

## Journal of Materials Chemistry A

### **ARTICLE**

#### **Transition Metal-Substituted Lead Halide Perovskite Absorbers**

M. D. Sampson, J.-S. Park, R. D. Schaller, M. K. Y. Chan, and A. B. F. Martinson and

Received 00th January 20xx, Accepted 00th January 20xx

DOI: 10.1039/x0xx000000x

www.rsc.org/

Lead halide perovskites have proven to be a versatile class of visible light absorbers that allow rapid access to the long minority carrier lifetimes and diffusion lengths desirable for traditional single-junction photovoltaics. We explore the extent to which the attractive features of these semiconductors may be extended to include an intermediate density of states, for future application in multi-level solar energy conversion systems capable of exceeding the Shockley-Queisser limit. We computationally and experimentally explore the substitution of transition metals on the Pb site of MAPbX<sub>3</sub> (MA = methylammonium, X = Br or Cl) to achieve a tunable density of states within the parent gap. Computational screening identified both Fe- and Co-substituted MAPbBr<sub>3</sub> as promising absorbers with a mid-gap density of states, and the later films were synthesized via conventional solution-based processing techniques. First-principles density functional theory (DFT) calculations support the existence of mid-gap states upon Co incorporation and enhanced sub-gap absorption, which are consistent with UV-visible-NIR absorption spectroscopy. Strikingly, steady state and time-resolved PL studies reveal no sign of self-quenching for Co-substitution up to 25%, which suggest this class of materials to be a worthy candidate for future application in intermediate band photovoltaics.

#### Introduction

Lead halide perovskite semiconductors have been extensively studied for a variety of optoelectronic applications, <sup>1-2</sup> including photovoltaics (PVs), <sup>3-9</sup> photodetectors, <sup>10-12</sup> and LEDs. <sup>13-17</sup> There has been considerable interest in these materials due to their tunable optical properties, large absorption coefficients, excellent mobilities, long excited state lifetimes, low cost, and simple synthesis via solution-based deposition techniques by which most are commonly formed. <sup>1</sup> Since the first report of these materials as light absorbers in single-junction photovoltaics in 2009, <sup>18</sup> power conversion efficiencies exceeding 20% have been realized and rationalized owing to their excellent photophysical properties. <sup>19-20</sup>

Intermediate band (IB) PVs are a class of multi-junction devices that have the theoretical potential to surpass the Shockley-Queissier limit for single p-n junction cells. <sup>21</sup> IB PVs require an IB material sandwiched between two conventional (n- and p-type) semiconductors, which serve as selective contacts to the conduction band (CB) and valence band (VB), respectively. These PVs are designed to retain the high output voltages characteristic of large band gap semiconductors, while harvesting more energy from the available solar spectrum by absorbing pairs of sub-band gap photons to produce additional high-energy carriers. Only a handful of

examples of materials that exhibit the properties necessary for IB PV operation have been reported to date. <sup>22-23</sup> Thus far, GaAs is the most successful parent material owing to its excellent photophysical properties, to which perovskite halides have been compared, as well as the ability to form quantum wells with smaller gap. While the GaAs-quantum wells operate as IB PVs, the contribution to the photocurrent enabled by the intermediate band is meager, as it is limited by the achievable spatial density of the structurally strained quantum wells. The band gap of GaAs is also not ideal, as the optimal total band gap of an IB material has been calculated to be approximately 2.0 eV, which is split by a mid-gap level into two sub-band gaps of approximately 0.7 eV and 1.3 eV (Fig. 1). <sup>22</sup> In this arrangement, the maximum photovoltage is the difference between the quasi-Fermi levels (i.e. the electrochemical

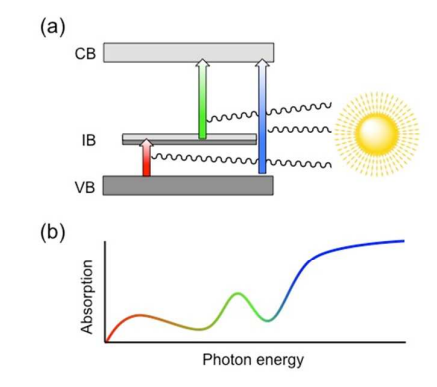


**Fig. 1** (a) Idealized schematic energy level diagram illustrating the working principle of an IB PV. (b) Corresponding idealized absorption spectrum of an IB PV.

<sup>&</sup>lt;sup>a.</sup> Materials Science Division, Argonne National Laboratory, Argonne, Illinois 60439, United States. E-mail: martinson@anl.gov

b. Center for Nanoscale Materials, Argonne National Laboratory, Argonne, Illinois 60439, United States. E-mail: mchan@anl.gov

<sup>†</sup> Electronic supplementary information (ESI) available. See DOI: 10.1039/x0xx00000x

potentials of the electrons) in the CB and VB of the n- and p-side electrodes (2.0 eV).

We propose lead halide perovskites as potential candidates for IB PVs due to their outstanding photophysical properties, likely structural tolerance for metal substitution, and tunable band gap. Compared to conventional inorganic binary semiconductors like GaAs (band gap = 1.4 eV), a large compositional space has been identified for APbX<sub>3</sub> perovskites (A = cations such as Cs<sup>+</sup>, methylammonium [MA], or formamidinium [FA] and X = Cl, Br, and/or I). We have identified MAPbBr<sub>3</sub> as a promising parent material with nearly ideal parent band gap (~2.2 eV)<sup>24</sup> and hypothesize that partial substitution of Pb for earth-abundant transition metals may provide stable mid-gap states with tunable energy level, while retaining many of the desirable optoelectronic attributes of the parent material.

Recently, Andalibi et al. reported a theoretical study describing Hg doping into MAPbl<sub>3</sub>, creating a fully-occupied, narrow IB approximately 0.5 eV above the valence band maximum (VBM). <sup>25</sup> In experimental studies, the only elements that have been substituted for Pb in APbX<sub>3</sub> are in the same group IV, Sn<sup>26-31</sup> and Ge, <sup>32-33</sup> closely-related (periodic table neighbors) Bi, <sup>34-35</sup> and transition metal Cu. <sup>36</sup> These alternatives have garnered interest as a compromise in order to avoid the toxicity of Pb but at the expense of stability and device performance relative to their Pb-containing analogues. <sup>37-39</sup> Recently, Bi has also been utilized in conjunction with Ag to form the double perovskite Cs<sub>2</sub>Ag<sup>1</sup>Bi<sup>III</sup>Br<sub>6</sub>, which exhibits an encouraging photoluminescence lifetime, but retains a single gap, and only in single crystal form. <sup>40</sup>

In order to screen the widest range of substitutional possibilities for Pb in APbX<sub>3</sub>, we have utilized computational high throughput screening with density functional theory (DFT) calculations to select promising substituents that might be incorporated into the hybrid perovskite halide framework. Our goals in this screening were to select substituents that will create a mid-bandgap density of states near the optimal energy for an intermediate band within the parent gap (1.3 eV from VBM or –0.7 eV from CB minimum [CBM]).<sup>41</sup> The details of the high throughput computational screening approach will be the focus of a separate report. DFT screening of over 60 elements for Pb-site substitution in the room temperature, cubic MAPbBr<sub>3</sub> perovskite structure revealed that both Fe and Co, among others, may be expected to produce states within the parent gap.

Here, we report the synthesis and characterization of Feand Co-substituted MAPbBr $_{3-\gamma}Cl_{\gamma}$  (i.e. MAPb $_{1-x}Fe_xBr_{3-\gamma}Cl_{\gamma}$  and MAPb $_{1-x}Fe_xBr_{3-\gamma}Cl_{\gamma}$ ) thin films, prepared via one-step solution processing. Thin films are characterized by X-ray diffraction (XRD), UV-Vis absorption spectroscopy, and photoluminescence (PL) spectroscopy to understand both the structural and photophysical dependences on the transition metal substitution level (x). DFT calculations predict minimal structural changes and near-zero thermodynamic penalty with 1/8 Fe or Co substitutions on the Pb site, indicating the feasibility of Fe and Co incorporation into the structural framework that is experimentally corroborated by XRD

measurements. Electronic structure calculations further show Fe- and Co-induced deep levels in the band gap that results in sub-gap absorption, consistent with UV-Vis results for the Co-substituted sample. Although predicted by computations, attempts to experimentally substitute with Fe did not produce sub-gap absorption. Finally, time-resolved photoluminescence reveals the potential for these materials in future IB PVs. The studies and findings reported here provide new insight into the development and implementation of perovskite halides for IB PVs.

#### Results and discussion

#### Thin film fabrication

Thin films of Fe- and Co-substituted MAPbBr $_{3-\gamma}Cl_{\gamma}$  (MAPb $_{1-x}Fe_xBr_{3-\gamma}Cl_{\gamma}$  and MAPb $_{1-x}Co_xBr_{3-\gamma}Cl_{\gamma}$ , pictures of Co samples in Fig. S1) were prepared on either fused quartz (FQ) or fluorine-doped tin oxide (FTO) by simple one-step spin coating, following a method adapted from previous reports (see Experimental section for complete details). Attempts to prepare Fe- or Co-substituted perovskite films via two-step deposition or adding solvents or other additives to single-step deposition did not result in any observable improvements in film morphology or grain size as compared to one-step deposition. Attempts were made to soak MAPbBr $_{1-\gamma}Cl_{\gamma}$  films in FeBr $_2$  or CoBr $_2$  solutions in isopropanol in order to explore the ability for transition metal substitution to occur in prefabricated films; however, in most cases, this resulted in destruction of the films.

Initially, Fe- and Co-substituted films were only prepared by substituting the Br-only parent material, MAPbBr<sub>3</sub>. Cl was later introduced in order to better support Fe<sup>2+</sup> and Co<sup>2+</sup> ions in the perovskite framework, as Cl is expected to give a more desirable perovskite 'tolerance factor' and 'octahedral factor'. <sup>43</sup> The Goldschmidt tolerance factor (*t*) for an ABX<sub>3</sub> perovskite is calculated as shown in eqn (1).

$$t = (r_A + r_X)/(2^{1/2}[r_B + r_X])$$
 (1)

Here,  $r_A$ ,  $r_B$ , and  $r_X$  are the ionic radii for the cation (A), metal (B), and halide (X) sites, respectively. The 'octahedral factor' ( $\mu$ ) is simply the ratio of the ionic radius of B and X atoms, and is calculated as shown in eqn (2).

$$\mu = r_B/r_X \tag{2}$$

Together, the tolerance factor and octahedral factor have been established as widely accepted metrics for determining perovskite stability. Perovskite halides possess tolerance and octahedral factors in the ranges of 0.813 – 1.107 and 0.442 – 0.895, respectively. <sup>43</sup> In qualitative terms, as Fe<sup>2+</sup> ( $r_{Fe}$  = 92 pm) and Co<sup>2+</sup> ( $r_{Co}$  = 90 pm) have a much smaller ionic radii than Pb<sup>2+</sup> ( $r_{Pb}$  = 129 pm), one would expect smaller Cl<sup>-</sup> ( $r_{Cl}$  = 181 pm) to better support Fe<sup>2+</sup> and Co<sup>2+</sup> in the *Pm-3m* perovskite structure as compared to Br<sup>-</sup> ( $r_{Br}$  = 196 pm). For Fe<sup>2+</sup>, t = 0.923 and 0.935 and  $\mu$  = 0.469 and 0.508 for Br<sup>-</sup> and Cl<sup>-</sup>, respectively. For Co<sup>2+</sup>, t = 0.930 and 0.942 and  $\mu$  = 0.459 and 0.497 for Br<sup>-</sup> and Cl<sup>-</sup>, respectively. For both Fe<sup>2+</sup> and Co<sup>2+</sup>, the octahedral factor for Br<sup>-</sup> yields a  $\mu$  on the border of predicted stability for perovskite halides.

This prediction is borne out in films of the mixed Br/Cl perovskite that appear more uniform by optical microscopy and SEM than Br-only perovskites; however, both Br-only and mixed halide films possess a homogeneous structure, as evidenced by X-ray diffraction (XRD) studies (*vide infra*). Additionally, all films displayed relatively uniform distributions of Fe<sup>2+</sup>/Co<sup>2+</sup>, Pb<sup>2+</sup>, and Br<sup>-</sup>/Cl<sup>-</sup>, both in the cross section of the films (see GDOES, Fig. S2 and S3) and across the planar direction of the films (see EDX maps, Fig. S4. We note that the exact stoichiometry of the films is difficult to determine. The relative ratios of the inorganic cations (Pb and Fe/Co) and the halides (Br and Cl) refer to the ratios of the precursors in solution prior to spin coating. It is possible that the final stoichiometry of each film is slightly different than the nominal values

#### Structural prediction and characterization

DFT calculations predict that 1/8 Co and Fe substitution for Pb in MAPbBr3 and MAPbBr3-vClv will not change the lattice constant appreciably, as summarized in Table 1. Using PBE, the optimized lattice constant of MAPbBr<sub>3</sub> is 6.065 Å with an insignificant change in lattice constant ( $\Delta_{lat}$  = -0.05% and -0.13 % for Co and Fe, respectively) to 6.062 and 6.057 Å upon Fe substitution  $(MAPb_{0.87}Co_{0.13}Br_3)$  $MAPb_{0.87}Fe_{0.13}Br_3$ ), respectively. Comparing calculations performed with and without spin-orbit coupling, the difference in lattice parameters changes upon doping is of order 0.1%. For Co, the lattice constant is also largely insensitive to the U value selected. U values of 3 and 7 eV result in lattice constants of 6.057 Å ( $\Delta_{lat}$  = -0.13 %) and 6.059 Å ( $\Delta_{lat}$  = -0.10 %), respectively. Similar behavior is also observed for MAPbBr<sub>1.5</sub>Cl<sub>1.5</sub>, which has a smaller lattice constant than MAPbBr<sub>3</sub>. In all calculations, the change of the lattice constant upon Co/Fe substitution is less than 0.3%, which will be shown to be consistent with experimental findings below.

Table 1 Optimized lattice constant of MAPb1-xMxBr3-yCly (M = Co, Fe) from DFT calculations.

Material	<i>U</i> for M 3 <i>d</i>	Lattice constant	Change in lattice
	(eV)	(Å)	constant $\Delta_{lat}$ (%)
MAPbBr <sub>3</sub>	N/A	6.065	
$MAPb_{0.87}Co_{0.13}Br_3$	0	6.062	-0.05
	3	6.057	-0.13
	7	6.059	-0.10
$MAPb_{0.87}Fe_{0.13}Br_3$	0	6.057	-0.13
MAPbBr <sub>1.5</sub> Cl <sub>1.5</sub>	N/A	5.933	
MAPb <sub>0.87</sub> Co <sub>0.13</sub> Br <sub>1.</sub>	0	5.916	-0.29
<sub>5</sub> Cl <sub>1.5</sub>			
	3	5.922	-0.19
	7	5.915	-0.30

All levels of Fe and Co substitution studied (x = 0.13 to 0.25 for Fe and x = 0.13 to 0.5 for Co) result in films that exhibit the anticipated room temperature cubic perovskite structure, *Pm-3m*, as evidence by XRD patterns in Fig. 2 and S5. For these experimental conditions, the observed reflections for each film

match that of the MAPbBr $_3$  parent material (Fig. 2a and S5). We find no evidence for free PbBr $_2$ /PbCl $_2$  or FeBr $_2$ /CoBr $_2$  for substitution levels from x = 0.13 to 0.5 (Fig. S6). Crystallinity of the films decreases considerably at substitution levels above x = 0.25, and thus, for simplicity, we have only included levels of Co substitution of x = 0.13 and 0.25 in these studies. As a control, we prepared a film consisting of a 1:1 ratio of CoBr $_2$  and MABr (i.e. substitution level of x = 1, no Pb), and this film no longer possesses the *Pm-3m* structure of room temperature MAPbBr $_3$  (Fig. S7). Fe substitution did not result in a sub-gap absorption feature (*vide infra*), and therefore, these films were not studied in further detail.

The lattice parameters and unit cell volume, deduced from the (100) reflection in XRD, for the set of MAPb<sub>1-x</sub>Co<sub>x</sub>Br<sub>3-v</sub>Cl<sub>v</sub> films varies from a = b = c = 5.884(1) - 5.806(1) Å and V = $203.7(1) - 195.7(1) \text{ Å}^3$  (x = 0, y = 0 to x = 0, y = 1.5, respectively). As has been previously discussed, 26, 44 the unit cell dimensions of perovskite halides are primarily dictated by the composition of halides and/or organic cations. 45 This effect is also observed for our MAPb<sub>1-x</sub>Co<sub>x</sub>Br<sub>3-y</sub>Cl<sub>y</sub> films, where 20 increases with increasing y/3 (Cl fraction) (Fig. 2c). Consistent with DFT calculations, incorporation of Co<sup>2+</sup> into the perovskite framework does not significantly change the dimensions of the unit cell. For mixed Sn/Pb perovskite halides, similar results were observed: the lattice parameter a changed from only 8.929 to 8.930 Å for MAPbl<sub>3</sub> and MASn<sub>0.25</sub>Pb<sub>0.75</sub>l<sub>3</sub>, respectively, despite a large decrease in ionic radius (although less drastic,  $r_{Sn} = 118 \text{ pm}$ ). For the Br-only perovskites, the lattice parameter and unit cell volume ranged from a = b = c = 5.884(1), 5.888(1), 5.888(1) Å and V = 203.7(1), 204.1(1), 204.1(1)  $\text{Å}^3$  for Co concentrations of x = 0, x = 0.13, and x = 0.25, respectively. Indeed, our studies further support that the unit cell dimensions of perovskite halides, if the phase does form, are primarily dictated by the nature of the halides and/or organic cations and are little affected by the nature of the inorganic B cation.

To compare crystallinity between samples, we calculated the full width at half maximum (FWHM) at the (200) reflection (see Fig. 2b) for each film. Others have utilized the Scherrer equation to quantify an average crystallite size for perovskite halides. 46-49 However, due to its dependence on film thickness, potential peak broadening due to crystal defects/strain, and the finite energy resolution of most lab X-ray sources, we believe that further interpretation beyond FWHM is premature, and therefore, we chose not to analyze our films with the Scherrer equation. As shown in Fig. 2d, FWHM increases (i.e. "crystallinity" decreases) with increasing Clcontent y/3. This effect is unexpected, as we hypothesized that incorporating  $Cl^-$  would form a more stable Pm-3m structure with Co<sup>2+</sup>, as determined by the tolerance and octahedral factors (vide supra). We note that this analysis is not quantitative and should be used solely for comparing general "crystallinity" between films in this study.

#### First principles thermodynamics

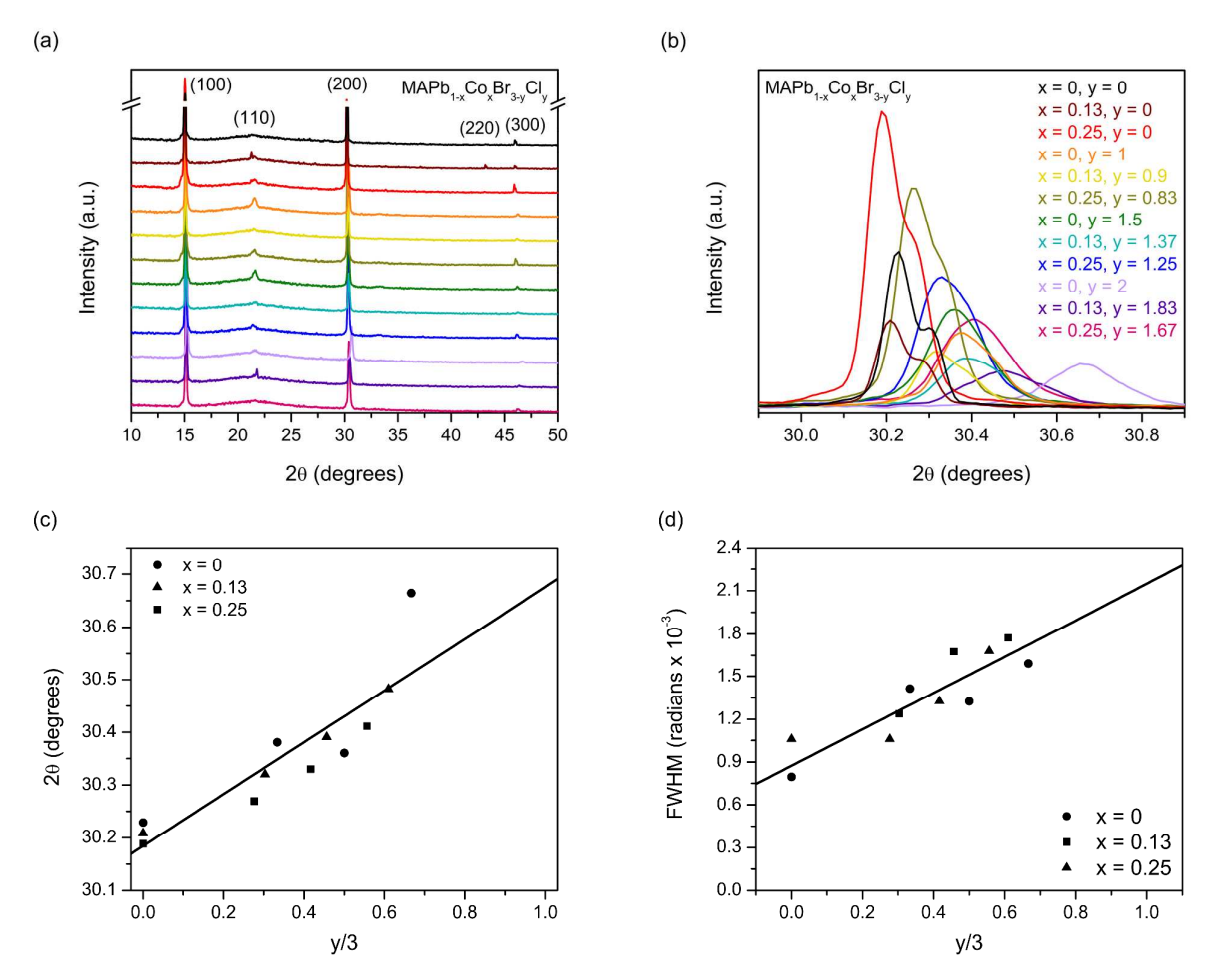


Fig. 2 (a) XRD patterns of  $MAPb_{1x}Co_xBr_{3y}Cl_y$  films. (b) Zoomed in region of the (200) XRD peak. (c) Reflection angle of the (200) XRD peak as a function of y/3 (Cl fraction) across all Co substitution levels. (d) FWHM of (200) XRD peak with increasing y/3. The lines are best linear fits to the data.

The thermodynamics of Co and Fe substitution is investigated using DFT energies of MAPbBr<sub>3</sub> and MAPb<sub>0.87</sub>M<sub>0.13</sub>Br<sub>3</sub> (M = Co or Fe). The formation energy for M incorporation, calculated against binary bromide formation, is shown in eqn (3).

$$\Delta E = \frac{E\left(MA_{8}Pb_{7}MBr_{24}\right) + E\left(PbBr_{3}\right) - 8E\left(MAPbBr_{3}\right) - E\left(MBr_{2}\right)}{8} + k_{B}T\left\{x\ln x + (1-x)\ln(1-x)\right\}$$
(3)

Here,  $k_{\rm B}$  is the Boltzmann constant, x is 1/8, and T is growth temperature (100 °C). The values of  $\Delta E$ , under different applied Hubbard U corrections for the Co d electrons, are shown in Table 2. For Co, the values of  $\Delta E$  are either similar or less than  $k_{\rm B}T$  at growth temperature (0.032 eV), or negative, indicating thermodynamic feasibility for Co incorporation into the MAPbBr<sub>3</sub> framework. Similar calculations were performed to investigate the thermodynamics of Co substitution in MAPbBr<sub>1.5</sub>Cl<sub>1.5</sub>, and the calculated values of  $\Delta E$  are similar to those in MAPbBr<sub>3</sub>. The formation energy,  $\Delta E$ , for Fe incorporation in MAPbBr<sub>3</sub> is 47 meV (U = 0 eV), slightly higher as compared to Co incorporation, indicating that the Fe incorporation is less favored.

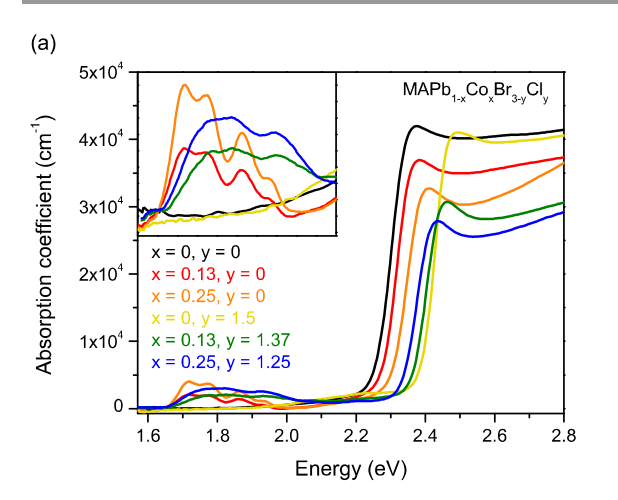
Table 2 Formation energy  $\Delta E$  for incorporation of M (M = Co, Fe) from DFT calculations.

Host material	M	<i>U</i> for M 3 <i>d</i> (eV)	ΔE (eV)
MAPbBr <sub>3</sub>	Co	0	0.036
		3	0.039
		7	-0.087
	Fe	0	0.047
$MAPbBr_{1.5}Cl_{1.5}$	Co	0	0.039
		3	0.040
		7	-0.100
MAPbBr <sub>3</sub>	Co	0	0.036
		3	0.039

#### Electronic structure and optical properties

Reflectance-corrected, steady state absorption spectra were obtained for the Fe- and Co-substituted MAPb<sub>1-x</sub>Fe<sub>x</sub>Br<sub>3-y</sub>Cl<sub>y</sub> and MAPb<sub>1-x</sub>Co<sub>x</sub>Br<sub>3-y</sub>Cl<sub>y</sub> films (Fig. 3a and S8). Fe substitution did not result in a sub-gap absorption feature (see Fig. S8), and therefore, these films were not further examined. For each Co-substituted film, the absorption spectrum shows a sharp band

edge and excitonic peak that is characteristic of MAPbBr<sub>3</sub> thin films. Band gaps extracted from Tauc plots display values of 2.27, 2.29, and 2.31 eV for  $MAPb_{1-x}Co_xBr_3$  (x = 0, 0.13, 0.25, respectively; see Fig. S9). The band gaps of the other MAPb<sub>1-</sub> <sub>x</sub>Co<sub>x</sub>Br<sub>1-v</sub>Cl<sub>v</sub> films corresponding to the absorption spectra shown in Fig. 3a are listed in Table S1. In addition to the band edge, Co-substituted samples display an additional sub-band gap absorption feature between 1.65 - 2.0 eV. This feature is made up of at least four closely spaced peaks and becomes broader with a shift to slightly higher energy in the Clcontaining films. The multiplet centered at ~1.8 eV is characteristic of CoBr<sub>2</sub> in a Br-rich environment, commonly represented as either  $[CoBr_4]^{2-}$  or  $[CoBr_6]^{4-50-51}$  For comparison, this feature is also present in a control sample of  $CoBr_2$  and MABr (no Pb, x = 1; see Fig. S10). However, the observation of a shift of this Co-related absorption in the Clcontaining films, as well as shift in band gap of the MAPbBr<sub>1.5</sub>Cl<sub>1.5</sub> film, in addition to a reduction in parent absorption intensity upon adding CoBr2, provide strong evidence that Co is chemically incorporated into the perovskite structure. This proportional change in maximum absorption



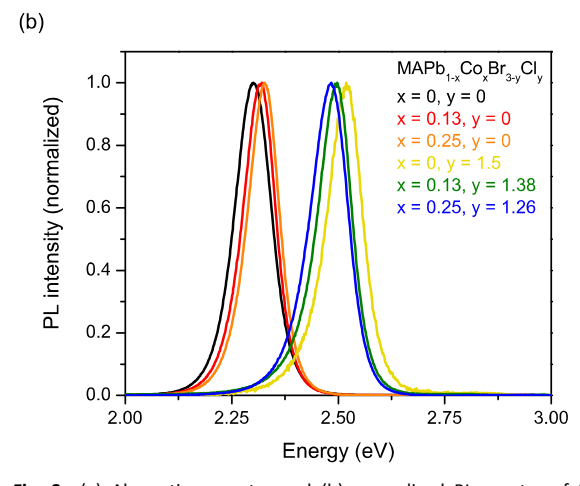
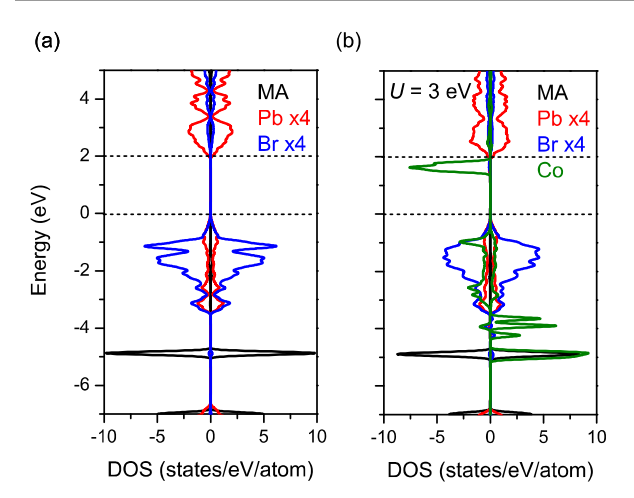


Fig. 3 (a) Absorption spectra and (b) normalized PL spectra of MAPb1-  $_x$ Co $_x$ Br3- $_y$ Cl $_y$  thin films.

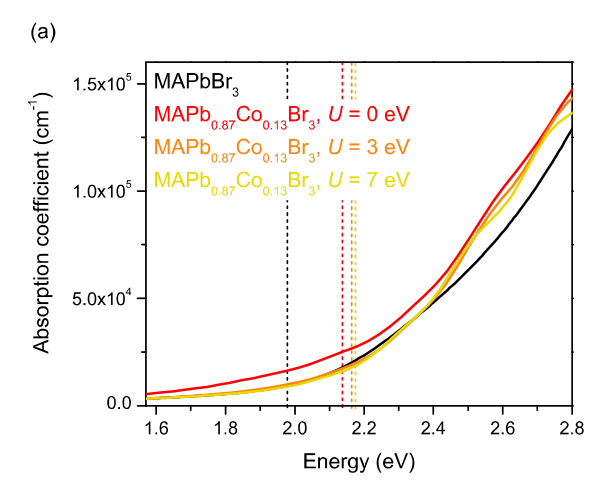
coefficient for both the parent perovskite band gap and the Co-based mid-gap states as a function of the amount of Co substitution is shown in Fig. S11. We observed no evidence for segregated states – such as Br- or Cl-phase separation – from the absorption spectra, in agreement with XRD. A second, even lower energy absorption is expected in the case of an IB material with ideal electronic doping in which the Fermi level lies within the IB (see Fig. 1). However, an additional absorption feature is not observed in the expected range from 0.5 – 0.7 eV upon UV-vis-NIR spectroscopy study out to 2500 nm (~0.5 eV). Therefore, we conclude that the mid-gap density of states are unfilled at the current electronic doping level, which is too small to measure with our Hall Measurement System (less than  $10^{16}$  cm<sup>-3</sup>) in both un- and Co-substituted thin films.

The DFT-computed electronic densities of states and absorption coefficient for MAPbBr<sub>3</sub>, MAPb<sub>0.87</sub>Co<sub>0.13</sub>Br<sub>3</sub>, MAPbBr<sub>1.5</sub>Cl<sub>1.5</sub>, and MAPb<sub>0.87</sub>Co<sub>0.13</sub>Br<sub>1.5</sub>Cl<sub>1.5</sub> are in reasonable agreement with those derived from experiment (see Fig. 4, 5, and S12). We find that PBE and PBE+U approximations both predict mid-gap states. The positions of the mid-gap states and the intensity of sub-gap absorption vary slightly with the value of U (Fig. 4, 5, S13, S14, and S15). In the DFT (PBE) calculation of MAPb<sub>0.87</sub>Co<sub>0.13</sub>Br<sub>3</sub>, there are three empty mid-gap states and two occupied levels in the parent band gap for the majority spin whereas there is no gap state for the minority spin (Fig. S13). Because of the mid-gap states, the absorption at relatively low energy is enhanced as compared to pure MAPbBr<sub>3</sub> and MAPbBr<sub>1.5</sub>Cl<sub>1.5</sub>. In the PBE+U calculations, on-site Coulomb potential increases (decreases) the position of the unoccupied (occupied) gap states. As a result, the occupied levels are all below the valence band maximum with U = 3 eV; however, three unoccupied levels remain in the band gap, as



**Fig. 4** Calculated electronic structure of (a) MAPbBr<sub>3</sub> and (b) MAPb<sub>0.87</sub>Co<sub>0.13</sub>Br<sub>3</sub>. In the calculations, a Hubbard U of 3 eV is used for Co d orbitals. The dashed horizontal lines represent the band edges of pure MAPbBr<sub>3</sub> estimated by the N 2s semicore level as reference in the calculations. The density of states of the Co-substituted system is broader than that of the pure system.

shown in Fig. 4. The mid-gap states are mainly composed of Co d orbitals, with a small amount of mixing from the Br p orbitals. As the unoccupied levels increase in energy with increasing U, photon transition energy is also increased, resulting in the reduced absorption at energy below the band gap (Fig. 5a and S15). When a strong Coulomb potential of U =7 eV is applied, the unoccupied levels becomes even higher than the conduction band minimum (Fig. S14), showing no extra gain in absorption at the lower energy, in contrast to the experiments. This indicates that U = 7 eV is too strong to model Co alloyed hybrid perovskites; we suggest the calculations without U (U = 0 eV) and with U = 3 eV to be regarded as bounds. In order to circumvent the errors often involved in predicting the energy eigenvalues of unoccupied states, we also calculated the energy gap of MAPbBr3 and MAPb<sub>0.87</sub>Co<sub>0.13</sub>Br<sub>3</sub> using the DFT total energy approach  $\Delta$ -sol<sup>52</sup> based on the principles of  $\Delta$ SCF. We verify that this approach reproduces the measured intermediate band energy level for



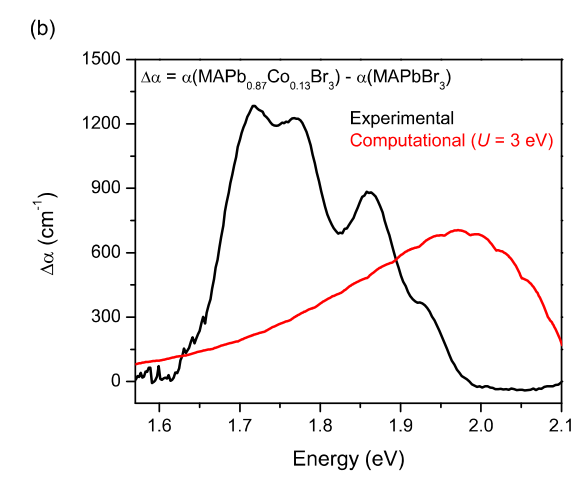


**Fig. 5** (a) Calculated absorption coefficient of MAPb<sub>0.87</sub>Co<sub>0.13</sub>Br<sub>3</sub> with U values (for Co 3d orbitals) of 0 (red), 3 (orange), and 7 eV (yellow) as compared to the calculated absorption coefficient of MAPbBr<sub>3</sub> (black). The calculated band gaps are indicated with vertical dotted lines. (b) Change in absorption coefficient ( $\Delta\alpha$ ) of MAPb<sub>0.87</sub>Co<sub>0.13</sub>Br<sub>3</sub> from MAPbBr<sub>3</sub> for experimental (black) and computations (red, U = 3 eV).

Mn in GaAs<sup>53</sup> (See Experimental Section for more details). The lowest intermediate band with respect to the VBM of MAPb<sub>0.87</sub>Co<sub>0.13</sub>Br<sub>3</sub> is calculated as 1.78 and 1.80 eV using U=0 and 3 eV, respectively. These values are clearly smaller than the energy gap of MAPbBr<sub>3</sub>, 2.24 eV, indicating that the Co induced states are in the band gap. The  $\Delta$ -sol prediction of the position of the lowest state within the gap is also largely independent of the value of U.

We find that Co incorporation also induces mid-gap states in the band gap of  $MAPb_{0.87}Co_{0.13}Br_{1.5}Cl_{1.5}$ . Similar to the bromide-only sample, three induced, unoccupied bands increase in energy as the U value increases, and thus, the extra absorption by Co incorporation is shifted to higher energy (Fig. S12 and S16). In contrast to Co substitution, computationally predicted mid-gap states for the Fe-substituted material,  $MAPb_{0.87}Fe_{0.13}Br_3$ , were not observed experimentally (Fig. S17 and S18). The fact that predicted intermediate bands for Fe were not observed may stem from an error in the position of these bands due to the uncertainty in describing the on-site Coulomb interaction, and/or the lack of Fe incorporation in the perovskite crystal structure due to less favorable thermodynamics as compared to Co. This matter is subject to further investigation.

The calculated band gap of MAPbBr<sub>3</sub> and MAPbBr<sub>1.5</sub>Cl<sub>1.5</sub> are 1.98 and 2.27 eV, respectively. As the band gap is increased by 0.3 eV with the introduction of CI, the absorption spectra are also shifted to higher energy. In addition, we find that Co substitution increases the energy of the parent gap in the bromide-only and mixed halide compounds by 0.18 eV and 0.03 eV, to 2.16 and 2.30 eV, respectively, when U = 3 eV is applied. An increase in parent gap with Co-doping is also observed in experimental UV-Vis and PL measurements of MAPbBr<sub>3</sub>-based samples (Fig. 3). The density of states at the bottom of the conduction band increases with Co incorporation, leading to increasing absorption above the band gap (2.1-2.6 eV in Fig. 5a). For better comparison with experimental results, difference plots of absorption coefficients between Co-substituted and pure (unsubstituted) systems are shown in Fig. 5b, S15, S16, and S19.

We note that the DFT electronic structure calculations presented have been performed without spin-orbit coupling (SOC). While SOC is important for Pb,<sup>54</sup> PBE+SOC largely underestimates the band gap by more than 1 eV due to typical DFT band gap errors with local and semilocal functionals.<sup>52</sup> We also find that SOC does not change the positions of the midgap states with respect to N semicore level.

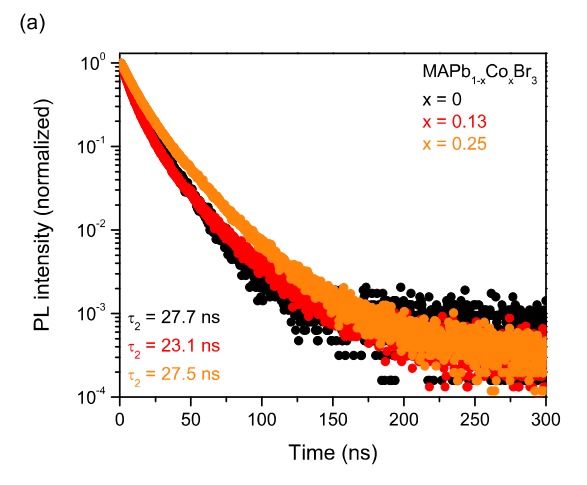
When U=3 eV is applied, the occupied Co levels are at least 2.5 eV lower than the lowest unoccupied level in the band gap, indicating that on-site optical transitions with subband gap photons are not possible. On the other hand, if U is not applied, d-d transitions are possible from 0.65 eV to 1.31 eV; however, these transitions are calculated to be weak.

These experimental and computational findings improve upon the work of Andalibi et al., which reports the computed electronic structure of Hg-doped MAPbl<sub>3</sub> (band gap = 1.5~1.6 eV). We note that this study differs in the perovskite system under investigation and reports only on a computational

modeling by DFT. Our study differs substantially in its investigation of substituting 3d transition metals with open shells in MAPbBr<sub>3</sub>. The Hg-induced IB has no s or p orbital character, indicating that it has mainly d and/or f orbital characters. The full d shell of Hg is more likely to be filled and therefore not as effective as an IB, compared to those introduced by the 3d dopants in the current study.

All of the Br-only perovskite films display intense steady state PL, which shifts to slightly higher energy upon substitution with Co (Fig. 3b and S20). This is perhaps the strongest evidence that Co must be substituting for Pb in the perovskite halide, as opposed to a mixed phase. The PL peak is centered at 2.30, 2.32, and 2.33 eV for  $MAPb_{1-x}Co_xBr_3$  x = 0, 0.13, and 0.25, respectively (Fig. 3b and Table S1). The increase in band gap is consistent with prediction, although of a smaller magnitude. These intense steady state PL measurements further suggest that the long excited state lifetimes that allow for radiative relaxation in the parent material may be largely preserved in the new alloy (vide infra). Cl incorporation significantly diminishes PL intensity. There are contradictory studies in the literature on the effect of CI incorporation on photoluminescence properties. Yan et al. conclude that Cl incorporation decreases PL intensity (as we observed), but can enhance PL intensity in a high MABr concentration environment. 55 Zhang et al. conclude that CI incorporation increases PL intensity; however, the significant enhancements are only observed for relatively low CI stoichiometry (y < 1.2). 56 The PL peaks for mixed Br/Cl perovskite films are shifted to higher energy, consistent with the shift in band gap. The PL peak is centered at 2.52, 2.50, and 2.48 eV for MAPbBr<sub>1.5</sub>Cl<sub>1.5</sub>,  $MAPb_{0.87}Co_{0.13}Br_{1.63}Cl_{1.37}$ and  $MAPb_{0.75}Co_{0.25}Br_{1.75}Cl_{1.25}$ , respectively (Fig. 3b and Table S1). For each set of films shown in Fig. 3b, substitution of Co for Pb in the perovskite framework results in increased PL intensity over the parent material (Fig. S20). Additionally, no PL features were observed for any films in the range of 1.6 - 2.0 eV, where we might expect to observe features from the Co-related mid-gap states. This suggests that, in its current state, the mid-gap states are inaccessible via relaxation from parent perovskite PL. No PL was observed for the films upon excitation with 1.6 - 1.9 eV light (energy equivalent to the Co-related mid-gap absorption, see Fig. 3a).

To determine the effect that Co substitution has on photoexcited carrier lifetimes, we obtained time-resolved PL data (Fig. 6). For each film studied, the PL intensity displays a decay that was sufficiently modeled by a two-component exponential (Fig. S21 and Table S2). For the Br-only containing perovskites, the first component possesses a lifetime of  $\tau_1$  = ~10 ns, and the second component possesses a lifetime of  $\tau_2$  = ~26 ns. Substitution with Co did not have a significant effect on either of these lifetimes for the Br-only films (Fig. 6a). For applications in IB PVs, it's important to retain the long-lived photoexcited state lifetimes inherent of perovskite films, and therefore, this result demonstrates promise for creating quality IB materials from the Co-substituted films if the occupation of the Co-based mid-gap states can be tuned. Mixed Br/Cl perovskites containing Co possess nearly a



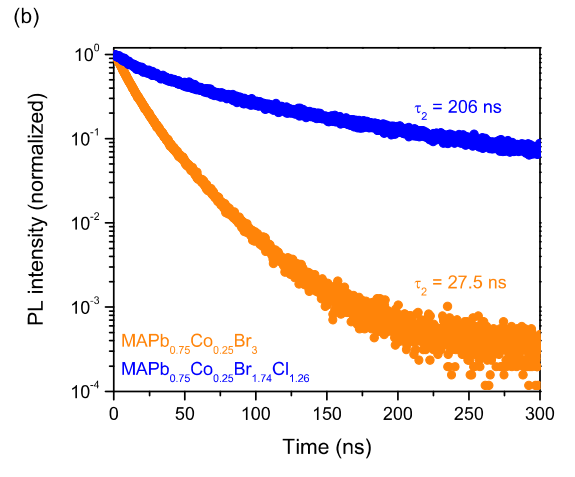


**Fig. 6** Time-resolved PL of (a) Br-only (y = 0) films revealing very little dependence on x, and (b) the halogen dependence on equally Cosubstituted (x = 0.25) films revealing a significant dependence on the Br/Cl ratio.

magnitude higher PL lifetime than Br-only films with an equivalent about of Co ( $\tau_2$  = 27.5 and 206 ns for MAPb<sub>0.75</sub>Co<sub>0.25</sub>Br<sub>3</sub> and MAPb<sub>0.75</sub>Co<sub>0.25</sub>Br<sub>1.75</sub>Cl<sub>1.25</sub>, respectively, Fig. 6b). Large-grain MAPbBr<sub>3</sub> films typically display lifetimes on the order of 100–200 ns;<sup>57</sup> however, multiple studies have reported similar values to the lifetimes we observe.<sup>40, 55</sup> Although our observed lifetime for MAPbBr<sub>3</sub> is slightly lower than some reports, the films are sufficient for direct comparison with Co-substituted samples. Our mixed Br/Cl perovskite films possess lifetimes in even better agreement with literature values for high-quality mixed halide films.<sup>56</sup> The increase in lifetime with Cl incorporation in our films is also consistent with previous reports.<sup>56</sup>

#### **Experimental**

#### Thin film fabrication

Thin films of Fe- and Co-substituted  $MAPb_{1-x}Br_{3-y}Cl_y$  were prepared by simple one-step solution spin coating, following a

method adapted from previous reports.<sup>42</sup> In each case, the appropriate ratio of 0.25 M MABr, MACl, PbBr<sub>2</sub>, PbCl<sub>2</sub>, FeBr<sub>2</sub>, and/or CoBr<sub>2</sub> was heated in dimethylformamide (DMF) at 100 °C for 4 hrs. An approximate 3% excess of MABr/MACI was added to each solution to ensure all PbBr2/PbCl2 was converted to perovskite. The appropriate substrate (fused quartz [FQ] or fluorine-doped tin oxide [FTO]) was pre-cleaned with a 10 min UV/ozone treatment and was then heated at 100 °C for 30 min before spin coating. Immediately before spin coating, the precursor solution was filtered and dropped onto the substrate. Films were spun at 2000 rpm for 30 sec followed by immediate annealing at 100 °C for 30 min. Films were stored in a dry, nitrogen-filled glovebox until further use. Sample thicknesses were measured using an Ambios Technology XP-1 stylus profilometer. The resulting films were typically between 200–300 nm thick by profilometry.

#### Characterization

XRD measurements were performed with a Bruker D2 Phaser diffractometer with Cu K $\alpha$  radiation. The scan range for  $2\theta$  was between 10 and 50° with a 0.01° step size and a time per scan of 0.05 s. Peak splitting observed in Fig. 2 is due to the XRD instrument not having a monochromator to filter out Cu KB irradiation. Therefore, both Cu  $K\alpha$  and  $K\theta$  irradiation are present in our XRD experiments, which cause the shoulders/doublets observed in Fig. 2. As such, we have no reason to believe these features are due to a secondary phase or any other materials characteristic. XRD patterns obtained on a different tool demonstrate the lack of shoulders/doublets (see Fig. S22). Glow discharge optical emission spectroscopy (GDOES) was performed with a Horiba GD-Profiler 2 spectrometer. Scanning electron microscopy (SEM) images were collected on a Hitachi S4700-II equipped with an energy dispersive X-ray (EDX) detector for elemental analysis. Optical absorption spectra were measured using a Varian Cary 5000 UV-Vis-NIR spectrophotometer equipped with an integrating sphere diffuse reflectance accessory. Absorption coefficients were calculated by correcting for the absorbance of the substrate, reflectance of the film, and the thickness of the film. Both steady state PL emission spectra and time-resolved PL, measured at the Center for Nanoscale Materials at Argonne National Laboratory, were obtained using a 405 nm, 35 ps pulse width diode laser operated at 1 MHz. PL signals were collected with a 75 mm focal length lens, passed through a 435 nm long pass filter, and directed onto a 0.3 m focal length spectrograph. Static PL spectra were collected with a cooled CCD, and time-resolved PL dynamics were recorded using an avalanche photodiode and time-correlated single photon counting electronics at specified emission wavelengths. Time constants for time-resolved PL were obtained by fitting PL decays to a bi-exponential function (I =  $A_1 \exp(-t/\tau_1) + A_2 \exp(-t/\tau_2)$  $t/\tau_2$ )) in Origin.

#### First principles modeling

To investigate the optoelectronic property of  $MAPb_{1-x}Co_xBr_3$ , calculations were performed within the density functional

theory (DFT) framework by using the generalized gradient approximation (GGA) parameterized by Perdew, Burke, and Ernzerhof (PBE) for the exchange correlation potential.<sup>58</sup> The projector-augmented wave (PAW) potentials were used, 59 as implemented in the VASP code. 60 The wavefunctions were expanded in plane waves with an energy cutoff of 500 eV. The atomic structures were fully relaxed until the residual forces were less than 0.03 eV/Å. Substitutional calculations were performed using 2×2×2 supercells of MAPbBr<sub>3</sub>, containing 96 atoms. For metal substitution calculations, one of the eight Pb atoms in the supercell was replaced with Fe or Co. For mixed Br/Cl calculations, a special quasi-random structure<sup>61</sup> was produced for the 96-atom supercell to model a solid solution on the anion site. Calculations were performed both with and without spin-orbit coupling. Absorption coefficients were calculated from the frequency-dependent dielectric function, obtained from summation over empty states. 62 We also note that advanced methods such as Bethe Salpeter Equation (BSE) calculations can be attempted to obtain more accurate absorption coefficients. For the relaxation and dielectric function calculations of the unit cell, 6×6×6 and 8×8×8 Monkhorst-Pack meshes were used for Brillouin zone integration, respectively. For the Brillouin zone integration of the supercell, 3×3×3 and 4×4×4 Monkhorst-Pack meshes were used, respectively.

Generally speaking, transition metal d bands are not accurately calculated in GGA calculations, and thus the effects of on-site Coulomb correlation, which has been described by a Hubbard-like (U) term, was examined. The implementation of Dudarev for the Hubbard *U* correction was used. 63 While the values of U for oxides have been calibrated to reproduce reaction energies derived from experimental enthalpies of formation,64 experimental data available bromides/chlorides are insufficient for this purpose. However, the appropriate value of *U* for Co oxides to reproduce reaction energies have been found to be 3.3-3.5 eV,64-65 and one expects the appropriate U values for chlorides and bromides to be lower than those for oxides. Our calculations for Co fluorides, CoF<sub>2</sub> and CoF<sub>3</sub>, show that a U value which reproduces the  $CoF_2 + \frac{1}{2} F_2 \leftrightarrow CoF_3$  reaction energy is in the range of  $0.3^2$  eV, indicating that the U value to reproduce energetic information for Co-bromides/chlorides is smaller than that for Co-oxides. On the other hand, we found that using U = 7 eV reproduces the optical absorption properties of  $CoBr_2$ , and in general the U values required to reproduce electronic structure properties at the single-particle level tend to be higher than those required to reproduce reaction energies. 66 Therefore, we performed the DFT+U calculations with U = 0, 3, and 7 eV. We acknowledge that  $Co^{2+}$  is a  $d^{7}$ transition metal and, since it resides in an octahedral environment in the perovskite lattice, is Jahn-Teller active.<sup>67</sup> Our calculations indicate that the high-spin states of these transition metals are energetically favored (0.66 eV and 1.55 eV lower per transition metal atom for Co<sup>2+</sup> and Fe<sup>2+</sup>, respectively) over the corresponding low-spin states. With a high-spin configuration, Co atoms are displaced from their ideal position, resulting in four shorter Co-Br bonds (~2.43 Å)

and two longer Co–Br bonds (~4.07 Å). Due to the local environment becoming more tetrahedral in character, there are two occupied levels and three unoccupied levels for the majority spin, as shown in Fig. 4. On the other hand, in the Fe substituted case, the lengthened and the shortened Fe–Br bonds are approximately 3.54 Å and 2.49 Å, respectively, indicating that the distortion of the Fe octahedra is smaller.

In order to calibrate the accuracy of DFT calculations for intermediate band levels, we performed DFT and DFT+ $\it U$ calculations (U = 0, 3 and 6 eV) to deduce position of the Mn level in Mn<sub>x</sub>GaAs. We found that both DFT and DFT+U predicts the Mn-derived impurity band above the GaAs VBM, at 0.32, 0.22, and 0.19 eV for U = 0, 3 and 6 eV, respectively, compared to the experimental value of 0.14 eV. In addition to considering the Kohn Sham eigenvalues corresponding to the Mn level, we also use the total energy approach  $\Delta$ -sol<sup>52</sup> in which the fundamental gap is calculated from E(N+1) + E(N-1)- 2E(N), where E(N) is the DFT total energy of a system with N electrons. Here, N is chosen to be the number of valence electrons in the 2×2×2 supercell. We find that the  $\Delta$ -sol value of the energy gap between the Mn level and VBM of Mn<sub>x</sub>Ga<sub>1-</sub>  $_{x}$ As is 0.26, 0.21, and 0.19 for U = 0, 3 and 6 eV, respectively, compared to the experimental value of 0.18 eV. Though far from a general proof, these results indicate that DFT and DFT+U calculations of intermediate band levels for a transition metal dopant in semiconductor are reasonably accurate using the  $\Delta$ -sol approach, which also shows weak dependence on the value of U.

#### **Conclusions**

The substitution of transition metals for Pb in ABX<sub>3</sub> hybrid perovskite halides was undertaken computationally and experimentally. DFT calculations predict a significant density of states may be generated between the parent compound valence band maximum and conduction band minimum with appropriate transition metal substitution - here Co and Fe. We find striking experimental evidence for Co incorporation of up to 25% of Pb sites with only small changes to crystal structure, lattice constants, or radiative recombination rate. Steady state absorption spectroscopy reveals a new apparently unfilled density of states that we hypothesize to be closer to the parent conduction band. As such, the substitutional alloy represents a promising new perovskite material with an additional mid-gap absorption, with potential application as a future IB absorber. Although proper IB principles require the IB to be half-filled, with further investigation into means of tuning the occupancy of the Co-related mid-gap states, a material may be realized suitable for use in an IB solar cell. Future studies should focus on moving the Fermi level into the intermediate band in order to achieve the second ground state sub-gap absorption required for efficient IB PV operation. These findings will be fundamental in the future design and implementation of perovskite materials as IB PVs, with the ultimate goal of attaining a single material capable of surpassing the Shockley-Queissier limit for single junction cells.

#### Acknowledgements

The research was performed at Argonne National Laboratory, a U.S. Department of Energy Office of Science Laboratory operated under contract no. DE-AC02-06CH11357 by UChicago Argonne, LLC. Use of the Center of Nanoscale Materials, an Office of Science user facility, was supported by the U.S. Department of Energy, Office of Science, Office of Basic Energy Sciences, under contract no. DE-AC02-06CH11357.

#### **Notes and references**

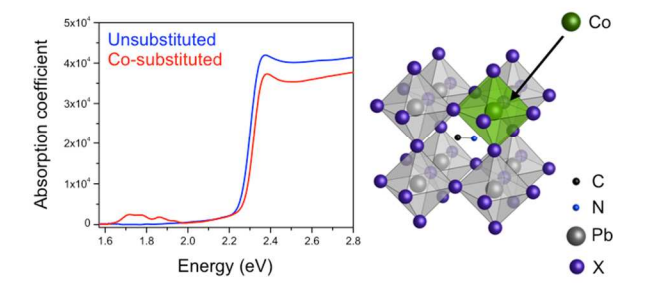
- J. S. Manser, J. A. Christians and P. V. Kamat, Chem. Rev., 2016, DOI: 10.1021/acs.chemrev.6b00136.
- Q. Chen, N. De Marco, Y. Yang, T.-B. Song, C.-C. Chen, H. Zhao, Z. Hong, H. Zhou and Y. Yang, *Nano Today*, 2015. 10, 355-396.
- J. Werner, C.-H. Weng, A. Walter, L. Fesquet, J. P. Seif,
   S. De Wolf, B. Niesen and C. Ballif, J. Phys. Chem. Lett.,
   2016, 7, 161-166.
- 4 M. M. Lee, J. Teuscher, T. Miyasaka, T. N. Murakami and H. J. Snaith, *Science*, 2012, **338**, 643-647.
- J. Burschka, N. Pellet, S.-J. Moon, R. Humphry-Baker, P. Gao, M. K. Nazeeruddin and M. Gratzel, *Nature*, 2013, 499, 316-319.
- H.-S. Kim, C.-R. Lee, J.-H. Im, K.-B. Lee, T. Moehl, A. Marchioro, S.-J. Moon, R. Humphry-Baker, J.-H. Yum, J. E. Moser, M. Grätzel and N.-G. Park, Sci. Rep., 2012, 2, 591.
- 7 C. Bi, Y. Yuan, Y. Fang and J. Huang, Adv. Energy Mater., 2015, 5, 1401616.
- D. P. McMeekin, G. Sadoughi, W. Rehman, G. E. Eperon, M. Saliba, M. T. Hörantner, A. Haghighirad, N. Sakai, L. Korte, B. Rech, M. B. Johnston, L. M. Herz and H. J. Snaith, *Science*, 2016, 351, 151-155.
- 9 C. D. Bailie, M. G. Christoforo, J. P. Mailoa, A. R. Bowring, E. L. Unger, W. H. Nguyen, J. Burschka, N. Pellet, J. Z. Lee, M. Gratzel, R. Noufi, T. Buonassisi, A. Salleo and M. D. McGehee, *Energy Environ. Sci.*, 2015, 8, 956-963.
- G. Maculan, A. D. Sheikh, A. L. Abdelhady, M. I. Saidaminov, M. A. Haque, B. Murali, E. Alarousu, O. F. Mohammed, T. Wu and O. M. Bakr, *J. Phys. Chem. Lett.*, 2015, 6, 3781-3786.
- 11 Q. Lin, A. Armin, P. L. Burn and P. Meredith, *Nature Photon.*, 2015, **9**, 687-694.
- 12 T. Moehl, J. H. Im, Y. H. Lee, K. Domanski, F. Giordano, S. M. Zakeeruddin, M. I. Dar, L.-P. Heiniger, M. K. Nazeeruddin, N.-G. Park and M. Grätzel, J. Phys. Chem. Lett., 2014, 5, 3931-3936.
- 13 C. C. Lin, A. Meijerink and R.-S. Liu, J. Phys. Chem. Lett., 2016, 7, 495-503.
- 14 X. Zhang, H. Lin, H. Huang, C. Reckmeier, Y. Zhang, W. C. H. Choy and A. L. Rogach, *Nano Lett.*, 2016, **16**, 1415-1420.
- 15 Y. Ling, Z. Yuan, Y. Tian, X. Wang, J. C. Wang, Y. Xin, K. Hanson, B. Ma and H. Gao, Adv. Mater., 2016, 28, 305-311.
- 16 S. Pathak, N. Sakai, F. Wisnivesky Rocca Rivarola, S. D. Stranks, J. Liu, G. E. Eperon, C. Ducati, K. Wojciechowski, J. T. Griffiths, A. A. Haghighirad, A. Pellaroque, R. H. Friend and H. J. Snaith, *Chem. Mater.*, 2015, 27, 8066-8075.
- 17 Z.-K. Tan, R. S. Moghaddam, M. L. Lai, P. Docampo, R. Higler, F. Deschler, M. Price, A. Sadhanala, L. M. Pazos,

- D. Credgington, F. Hanusch, T. Bein, H. J. Snaith and R. H. Friend, *Nature Nano.*, 2014, **9**, 687-692.
- 18 A. Kojima, K. Teshima, Y. Shirai and T. Miyasaka, J. Am. Chem. Soc., 2009, 131, 6050-6051.
- 19 National Renewable Energy Laboratory, Best Research-Cell Efficiencies, http://www.nrel.gov/pv/assets/images/efficiency\_char t.ipg, accessed: October, 2016.
- 20 H.-S. Kim, C.-R. Lee, J.-H. Im, K.-B. Lee, T. Moehl, A. Marchioro, S.-J. Moon, R. Humphry-Baker, J.-H. Yum, J. E. Moser, M. Grätzel and N.-G. Park, *Scientific Reports*, 2012, 2, 591.
- 21 Y. Okada, N. J. Ekins-Daukes, T. Kita, R. Tamaki, M. Yoshida, A. Pusch, O. Hess, C. C. Phillips, D. J. Farrell, K. Yoshida, N. Ahsan, Y. Shoji, T. Sogabe and J.-F. Guillemoles, *Appl. Phys. Rev.*, 2015, **2**, 021302.
- 22 A. Luque, A. Marti and C. Stanley, *Nature Photon.*, 2012, 6, 146-152.
- 23 A. Luque, A. Martí, C. Stanley, N. López, L. Cuadra, D. Zhou, J. L. Pearson and A. McKee, *J. Appl. Phys.*, 2004, 96, 903-909.
- 24 E. Edri, S. Kirmayer, D. Cahen and G. Hodes, *J. Phys. Chem. Lett.*, 2013, **4**, 897-902.
- 25 S. Andalibi, A. Rostami, G. Darvish and M. K. Moravvej-Farshi, Opt. Quant. Electron., 2016, 48, 258.
- 26 C. C. Stoumpos, C. D. Malliakas and M. G. Kanatzidis, *Inorg. Chem.*, 2013, **52**, 9019-9038.
- 27 F. Hao, C. C. Stoumpos, R. P. H. Chang and M. G. Kanatzidis, J. Am. Chem. Soc., 2014, 136, 8094-8099.
- 28 S. J. Lee, S. S. Shin, Y. C. Kim, D. Kim, T. K. Ahn, J. H. Noh, J. Seo and S. I. Seok, *J. Am. Chem. Soc.*, 2016, **138**, 3974-3977.
- 29 T. C. Jellicoe, J. M. Richter, H. F. J. Glass, M. Tabachnyk, R. Brady, S. E. Dutton, A. Rao, R. H. Friend, D. Credgington, N. C. Greenham and M. L. Böhm, J. Am. Chem. Soc., 2016, 138, 2941-2944.
- 30 K. P. Marshall, R. I. Walton and R. A. Hatton, *J. Mater. Chem. A*, 2015, **3**, 11631-11640.
- 31 F. Hao, C. C. Stoumpos, D. H. Cao, R. P. H. Chang and M. G. Kanatzidis, *Nature Photon.*, 2014, **8**, 489-494.
- 32 C. C. Stoumpos, L. Frazer, D. J. Clark, Y. S. Kim, S. H. Rhim, A. J. Freeman, J. B. Ketterson, J. I. Jang and M. G. Kanatzidis, *J. Am. Chem. Soc.*, 2015, **137**, 6804-6819.
- 33 T. Krishnamoorthy, H. Ding, C. Yan, W. L. Leong, T. Baikie, Z. Zhang, M. Sherburne, S. Li, M. Asta, N. Mathews and S. G. Mhaisalkar, *J. Mater. Chem. A*, 2015, **3**, 23829-23832.
- 34 B.-W. Park, B. Philippe, X. Zhang, H. Rensmo, G. Boschloo and E. M. J. Johansson, Adv. Mater., 2015, 27, 6806-6813.
- T. Singh, A. Kulkarni, M. Ikegami and T. Miyasaka, ACS Appl. Mater. Inter., 2016, 8, 14542-14547.
- 36 D. Cortecchia, H. A. Dewi, J. Yin, A. Bruno, S. Chen, T. Baikie, P. P. Boix, M. Grätzel, S. Mhaisalkar, C. Soci and N. Mathews, *Inorg. Chem.*, 2016, 55, 1044-1052.
- 37 Y. Takahashi, R. Obara, Z.-Z. Lin, Y. Takahashi, T. Naito, T. Inabe, S. Ishibashi and K. Terakura, *Dalton Trans.*, 2011, **40**, 5563-5568.
- 38 Y. Takahashi, H. Hasegawa, Y. Takahashi and T. Inabe, J. Solid State Chem., 2013, 205, 39-43.
- 39 M. H. Kumar, S. Dharani, W. L. Leong, P. P. Boix, R. R. Prabhakar, T. Baikie, C. Shi, H. Ding, R. Ramesh, M. Asta, M. Graetzel, S. G. Mhaisalkar and N. Mathews, Adv. Mater., 2014, 26, 7122-7127.
- A. H. Slavney, T. Hu, A. M. Lindenberg and H. I. Karunadasa, J. Am. Chem. Soc., 2016, 138, 2138-2141.
- 41 S. P. Bremner, M. Y. Levy and C. B. Honsberg, *Appl. Phys. Lett.*, 2008, **92**.

- 42 J.-Y. Jeng, Y.-F. Chiang, M.-H. Lee, S.-R. Peng, T.-F. Guo, P. Chen and T.-C. Wen, Adv. Mater., 2013, 25, 3727-3732.
- 43 C. Li, X. Lu, W. Ding, L. Feng, Y. Gao and Z. Guo, *Acta Crystallogr. Sect. B*, 2008, **64**, 702-707.
- 44 S. J. Clark, J. D. Donaldson and J. A. Harvey, J. Mater. Chem., 1995, 5, 1813-1818.
- 45 F. C. Hanusch, E. Wiesenmayer, E. Mankel, A. Binek, P. Angloher, C. Fraunhofer, N. Giesbrecht, J. M. Feckl, W. Jaegermann, D. Johrendt, T. Bein and P. Docampo, J. Phys. Chem. Lett., 2014, 5, 2791-2795.
- 46 B. D. Cullity and S. R. Stock, *Elements of X-ray Diffraction*, Prentice Hall, Upper Saddle River, NJ, 2001.
- 47 P. Jin Kyoung, H. Jin Hyuck, H. Hye Ji, L. Min Ho, S. Dae Ho, Y. Myoung Sang, S. Shi-Joon, K. Dae-Hwan and I. Sang Hyuk, *Nanotechnology*, 2016, **27**, 024004.
- 48 J. H. Heo, M. H. Lee, M. H. Jang and S. H. Im, *J. Mater. Chem. A*, 2016, **4**, 17636-17642.
- 49 W. Zhang, M. Saliba, D. T. Moore, S. K. Pathak, M. T. Hörantner, T. Stergiopoulos, S. D. Stranks, G. E. Eperon, J. A. Alexander-Webber, A. Abate, A. Sadhanala, S. Yao, Y. Chen, R. H. Friend, L. A. Estroff, U. Wiesner and H. J. Snaith, *Nature Commun.*, 2015, 6, 6142.
- 50 D. A. Fine, J. Am. Chem. Soc., 1962, 84, 1139-1144.
- 51 G. Stanescu and A. Trutia, Rom. Rep. Phys., 2005, 57, 2230228.
- 52 M. K. Y. Chan and G. Ceder, Phys. Rev. Lett., 2010, 105, 196403.
- 53 M. Linnarsson, E. Janzén, B. Monemar, M. Kleverman and A. Thilderkvist, *Phys. Rev. B*, 1997, **55**, 6938-6944.
- 54 J. Even, L. Pedesseau, J.-M. Jancu and C. Katan, *J. Phys. Chem. Lett.*, 2013, **4**, 2999-3005.
- 55 H. He, Q. Yu, H. Li, J. Li, J. Si, Y. Jin, N. Wang, J. Wang, J. He, X. Wang, Y. Zhang and Z. Ye, *Nature Commun.*, 2016, 7.
- 56 M. Zhang, H. Yu, M. Lyu, Q. Wang, J.-H. Yun and L. Wang, Chem. Commun., 2014, 50, 11727-11730.
- 57 D. Shi, V. Adinolfi, R. Comin, M. Yuan, E. Alarousu, A. Buin, Y. Chen, S. Hoogland, A. Rothenberger, K. Katsiev, Y. Losovyj, X. Zhang, P. A. Dowben, O. F. Mohammed, E. H. Sargent and O. M. Bakr, *Science*, 2015, **347**, 519-522.
- 58 J. P. Perdew, K. Burke and M. Ernzerhof, *Phys. Rev. Lett.*, 1996, **77**, 3865-3868.
- 59 P. E. Blöchl, Phys. Rev. B, 1994, 50, 17953-17979.
- G. Kresse and J. Furthmüller, Phys. Rev. B, 1996, 54, 11169-11186.
- 61 A. van de Walle, P. Tiwary, M. de Jong, D. L. Olmsted, M. Asta, A. Dick, D. Shin, Y. Wang, L. Q. Chen and Z. K. Liu, *Calphad*, 2013, **42**, 13-18.
- 62 M. Gajdoš, K. Hummer, G. Kresse, J. Furthmüller and F. Bechstedt, *Phys. Rev. B*, 2006, **73**, 045112.
- 63 S. L. Dudarev, G. A. Botton, S. Y. Savrasov, C. J. Humphreys and A. P. Sutton, *Phys. Rev. B*, 1998, **57**, 1505-1509.
- 64 Z. Zeng, M. K. Y. Chan, Z.-J. Zhao, J. Kubal, D. Fan and J. Greeley, J. Phys. Chem. C, 2015, 119, 18177-18187.
- 65 L. Wang, T. Maxisch and G. Ceder, *Phys. Rev. B*, 2006, 73, 195107.
- 66 B. Himmetoglu, A. Floris, S. de Gironcoli and M. Cococcioni, Int. J. Quantum Chem., 2014, 114, 14-49.
- 67 H. A. Jahn and E. Teller, Proc. Roy. Soc. A, 1937, 161, 220.

68

Cobalt substituted MAPbBr $_3$  films are a novel perovskite material with tunable midgap density of states providing promise for IB photovoltaics.



## **Supporting Information**

### **Transition Metal-Substituted Lead Halide Perovskite Absorbers**

M. D. Sampson, J.-S. Park, R. D. Schaller, M. K. Y. Chan,\* and A. B. F. Martinson\*

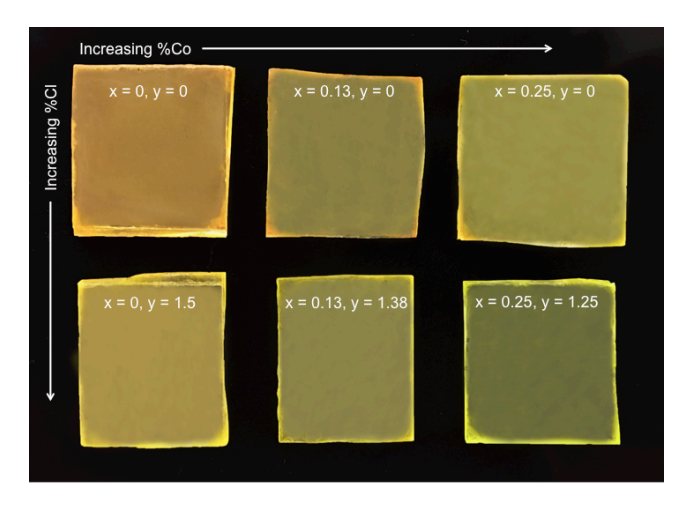


**Figure S1**. Photograph of MAPb<sub>1-x</sub>Co<sub>x</sub>Br<sub>3-y</sub>Cl<sub>y</sub> thin films on FQ.

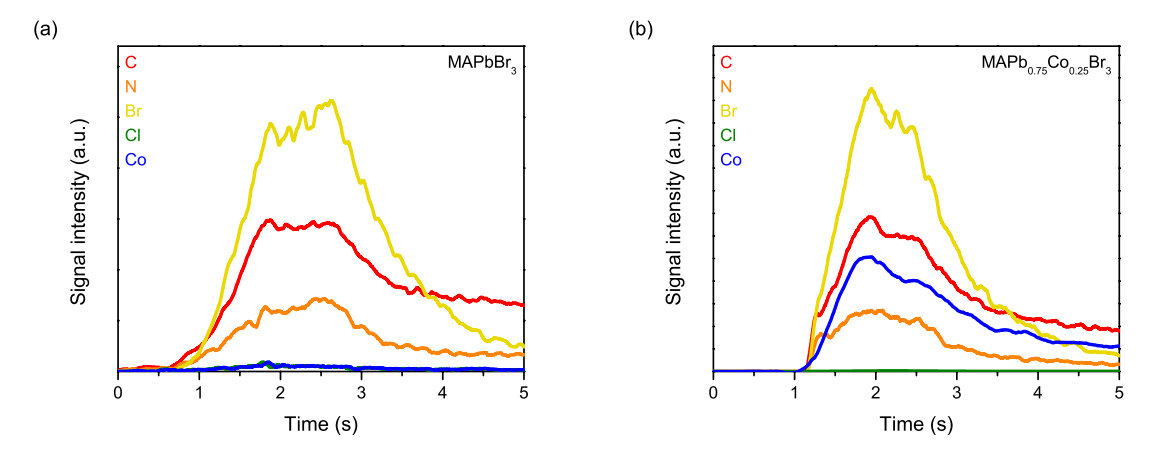


**Figure S2.** Glow discharge optical emission spectroscopy (GDOES) of (a) MAPbBr<sub>3</sub> and (b) MAPb<sub>0.75</sub>Co<sub>0.25</sub>Br<sub>3</sub> thin films. The signals for oxygen and hydrogen have been omitted for clarity.

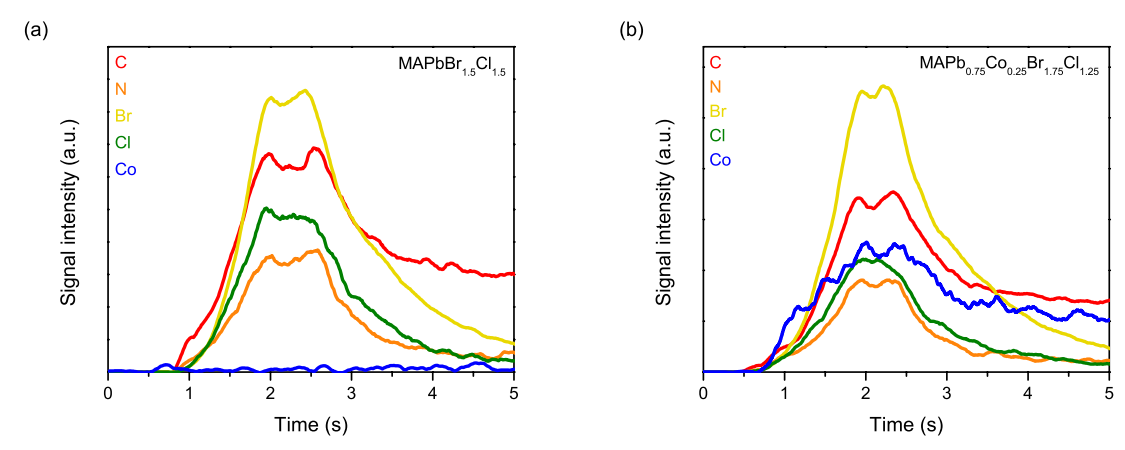


**Figure S3.** Glow discharge optical emission spectroscopy (GDOES) of (a) MAPbBr<sub>1.5</sub>Cl<sub>1.5</sub> and (b) MAPb<sub>0.75</sub>Co<sub>0.25</sub>Br<sub>1.75</sub>Cl<sub>1.25</sub> thin films. The signals for oxygen and hydrogen have been omitted for clarity.

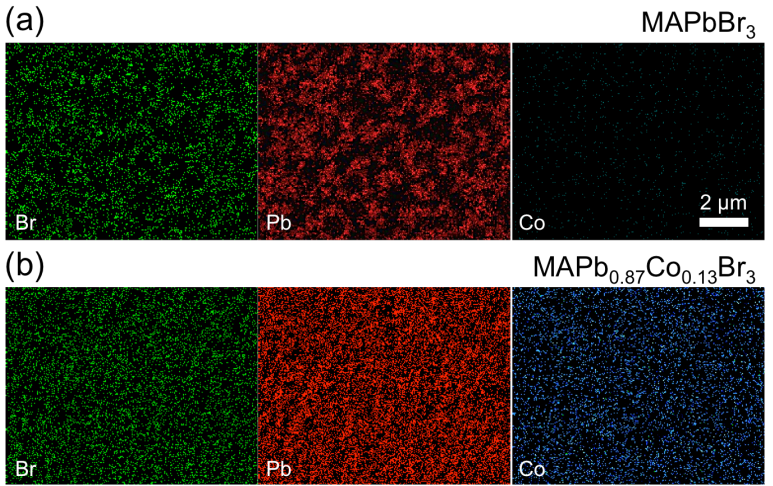


**Figure S4.** EDX elemental mapping of (a) MAPbBr<sub>3</sub> and (b) MAPb<sub>0.87</sub>Co<sub>0.13</sub>Br<sub>3</sub> thin films under the same data acquisition parameters. Green = Br, red = Pb, and blue = Co.

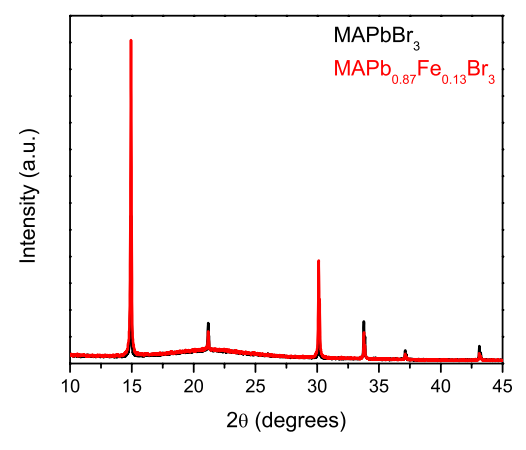


**Figure S5.** XRD patterns of MAPbBr<sub>3</sub> (black) and Fe-substituted MAPb<sub>0.87</sub>Fe<sub>0.25</sub>Br<sub>3</sub> (red) thin films.

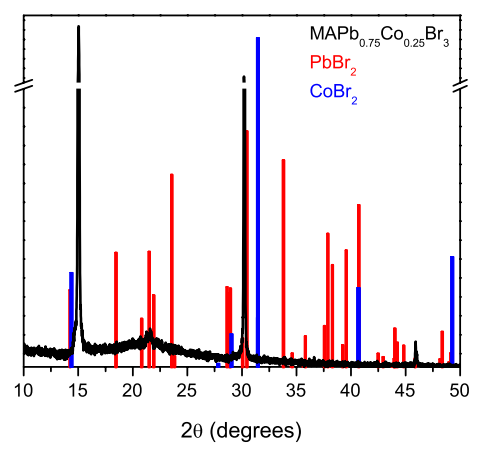


**Figure S6.** Predicted XRD patterns for PbBr<sub>2</sub> (red) and CoBr<sub>2</sub> (blue), with the XRD pattern for a MAPb<sub>0.75</sub>Co<sub>0.25</sub>Br<sub>3</sub> (black) thin film shown for comparison.

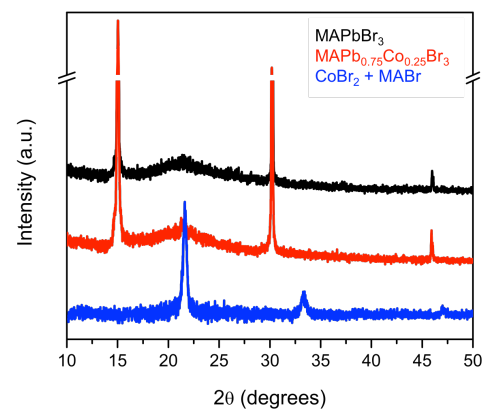


**Figure S7.** XRD pattern of a control film consisting of a 1:1 ratio of CoBr<sub>2</sub> to MABr (blue), with XRD patterns for MAPbBr<sub>3</sub> (black) and MAPb<sub>0.75</sub>Co<sub>0.25</sub>Br<sub>3</sub> (red) thin films shown for comparison.

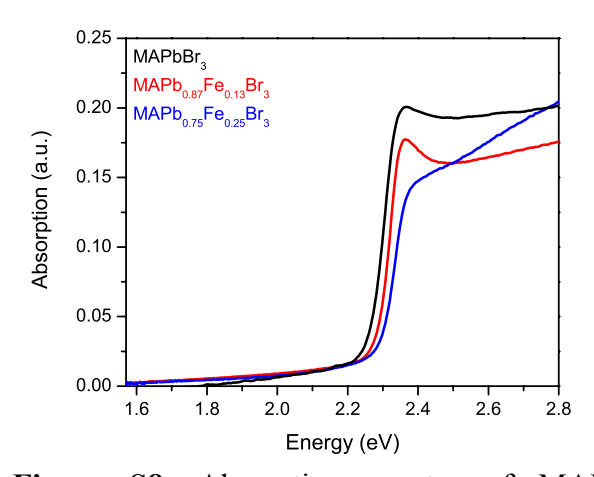


**Figure S8.** Absorption spectra of MAPbBr<sub>3</sub> (black), MAPb<sub>0.87</sub>Fe<sub>0.13</sub>Br<sub>3</sub> (red), and MAPb<sub>0.75</sub>Fe<sub>0.25</sub>Br<sub>3</sub> (blue) thin films, showing no mid-band gap absorption.

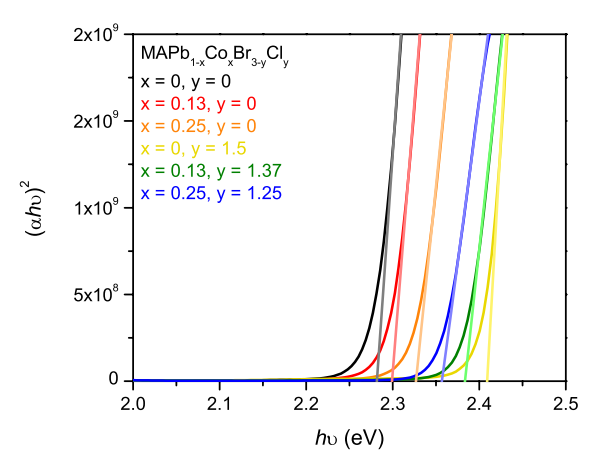


**Figure S9.** Tauc plots of the band gap for MAPb<sub>1-x</sub>Co<sub>x</sub>Br<sub>3-y</sub>Cl<sub>y</sub> thin films on FQ.

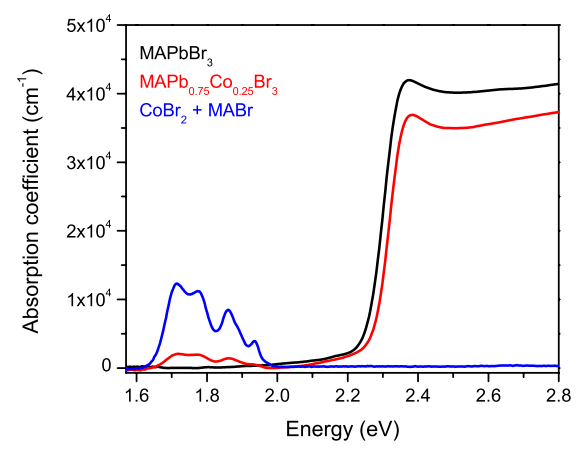


**Figure S10.** Absorption spectrum of a control film consisting of a 1:1 ratio of CoBr<sub>2</sub> to MABr (blue), with the absorption spectra for MAPbBr<sub>3</sub> (black) and MAPb<sub>0.75</sub>Co<sub>0.25</sub>Br<sub>3</sub> (red) thin films shown for comparison.

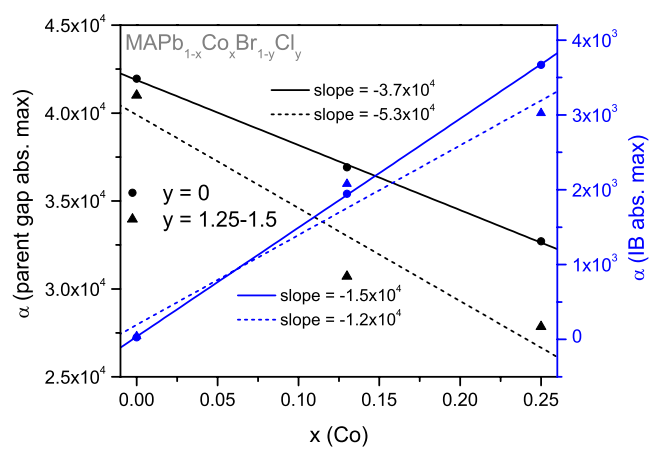


**Figure S11.** Peak absorption coefficient ( $\alpha$ ) for the parent gap (left axis) and Co-based midgap states (right axis) as a function of the amount of Co in the substituted film (x) for MAPb<sub>1-x</sub>Co<sub>x</sub>Br<sub>1-y</sub>Cl<sub>y</sub>. Linear fits of the data are shown to indicate trends.

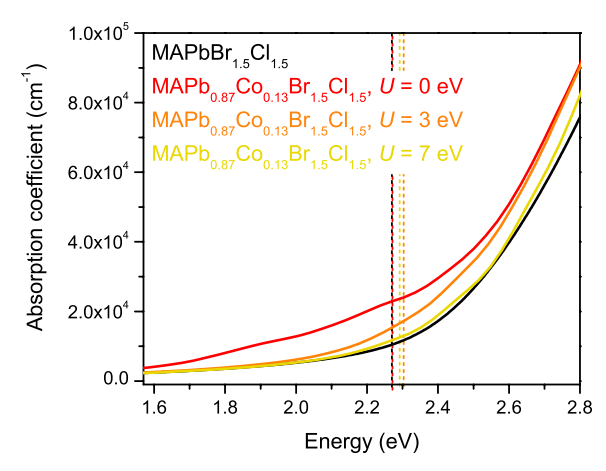


**Figure S12.** Calculated absorption coefficient of MAPb<sub>0.87</sub>Co<sub>0.13</sub>Br<sub>1.5</sub>Cl<sub>1.5</sub> with *U* values (for Co 3*d* orbitals) of 0 (red), 3 (orange), and 7 eV (yellow) as compared to the calculated absorption coefficient of MAPbBr<sub>1.5</sub>Cl<sub>1.5</sub> (black). The calculated band gaps are indicated with vertical dotted lines.

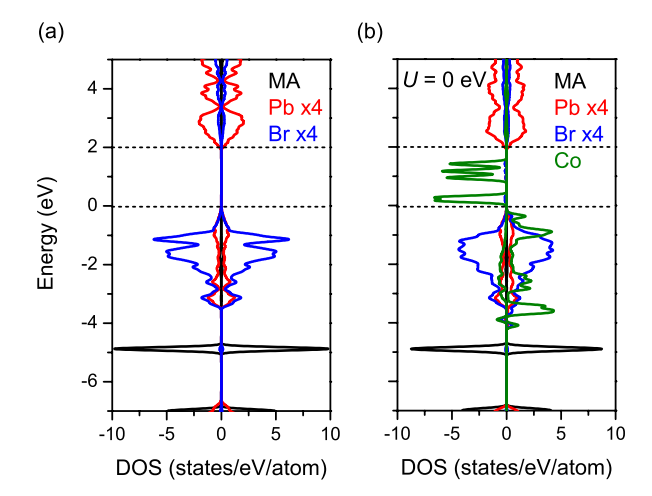


**Figure S13.** Calculated electronic structure of (a) MAPbBr<sub>3</sub> and (b) MAPb<sub>0.87</sub>Co<sub>0.13</sub>Br<sub>3</sub> with a Hubbard U = 0 eV used for Co d orbitals. The dashed horizontal lines represent the band edges of pure MAPbBr<sub>3</sub> estimated by N core level as reference in the calculations.

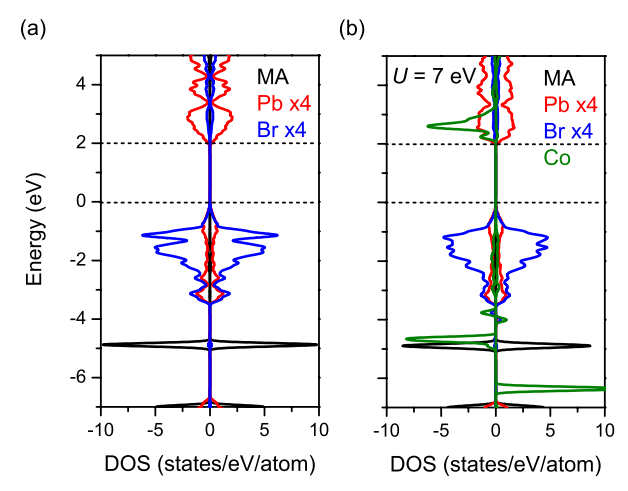


**Figure S14.** Calculated electronic structure of (a) MAPbBr<sub>3</sub> and (b) MAPb<sub>0.87</sub>Co<sub>0.13</sub>Br<sub>3</sub> with a Hubbard U = 7 eV used for Co d orbitals. The dashed horizontal lines represent the band edges of pure MAPbBr<sub>3</sub> estimated by N core level as reference in the calculations.

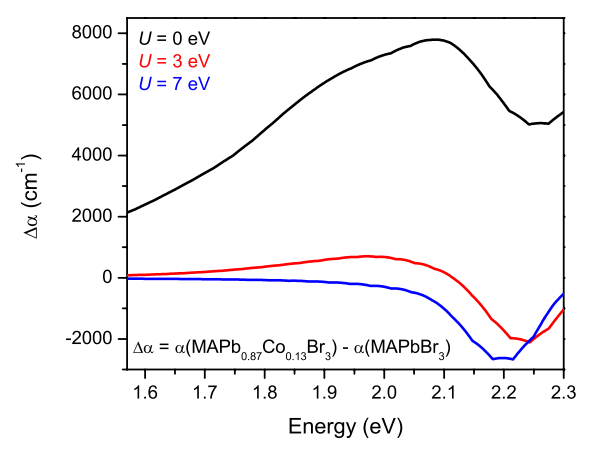


**Figure S15.** Change in absorption coefficient ( $\Delta \alpha$ ) of MAPb<sub>0.87</sub>Co<sub>0.13</sub>Br<sub>3</sub> from MAPbBr<sub>3</sub> for *U* values (for Co 3*d* orbitals) of 0 (black), 3 (red), and 7 eV (blue).

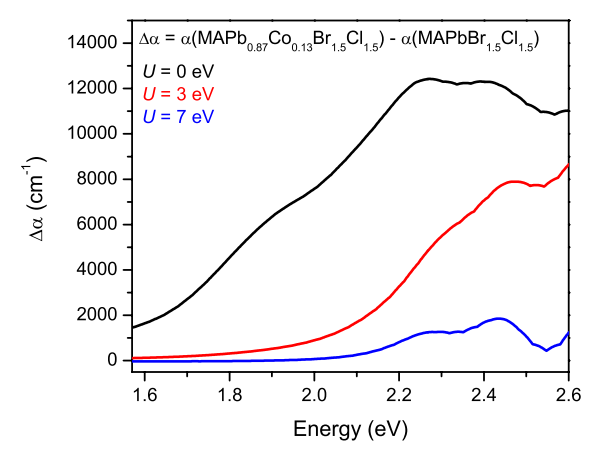


**Figure S16.** Change in absorption coefficient ( $\Delta\alpha$ ) of MAPb<sub>0.87</sub>Co<sub>0.13</sub>Br<sub>1.5</sub>Cl<sub>1.5</sub> from MAPbBr<sub>1.5</sub>Cl<sub>1.5</sub> for *U* values (for Co 3*d* orbitals) of 0 (black), 3 (red), and 7 eV (blue).

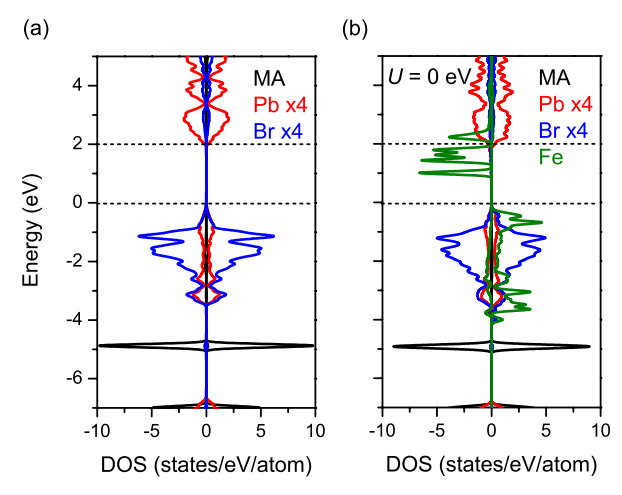


**Figure S17.** Calculated electronic structure of (a) MAPbBr<sub>3</sub> and (b) MAPb<sub>0.87</sub>Fe<sub>0.13</sub>Br<sub>3</sub> with a Hubbard U = 0 eV used for Fe d orbitals. The dashed horizontal lines represent the band edges of pure MAPbBr<sub>3</sub> estimated by N core level as reference in the calculations.

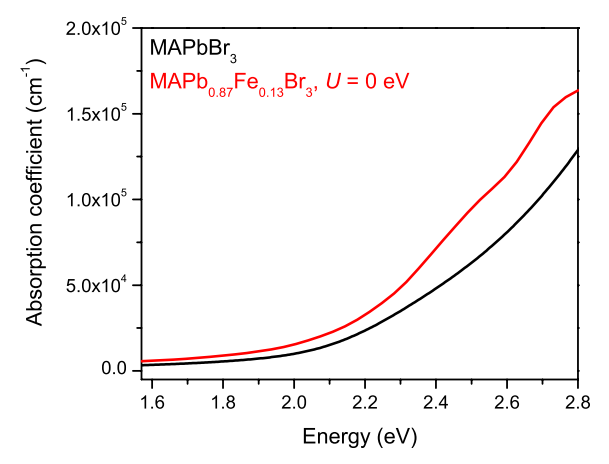


**Figure S18.** Calculated absorption coefficient of MAPb<sub>0.87</sub>Fe<sub>0.13</sub>Br<sub>3</sub> with a Hubbard U = 0 eV used for Fe d orbitals (red) as compared to the calculated absorption coefficient of MAPbBr<sub>3</sub> (black).

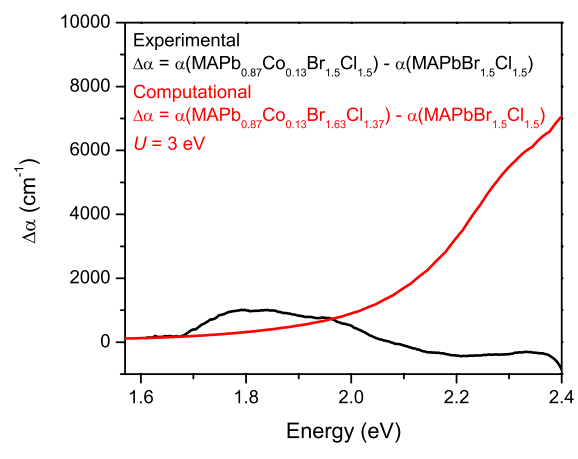


**Figure S19.** Change in absorption coefficient ( $\Delta \alpha$ ) of MAPb<sub>0.87</sub>Co<sub>0.13</sub>Br<sub>1.5</sub>Cl<sub>1.5</sub> from MAPbBr<sub>1.5</sub>Cl<sub>1.5</sub> for experimental (black) and computations (red, U = 3 eV). The experimental difference plot has a Br and Cl content of Br<sub>1.63</sub>Cl<sub>1.37</sub>.

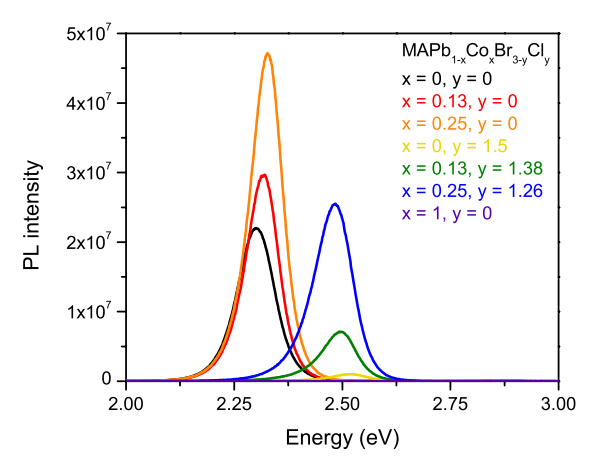


**Figure S20.** Non-normalized steady state PL spectra of of MAPb<sub>1-x</sub>Co<sub>x</sub>Br<sub>3-y</sub>Cl<sub>y</sub> thin films. The spectrum of a control film consisting of a 1:1 ratio of CoBr<sub>2</sub> to MABr is shown in purple.

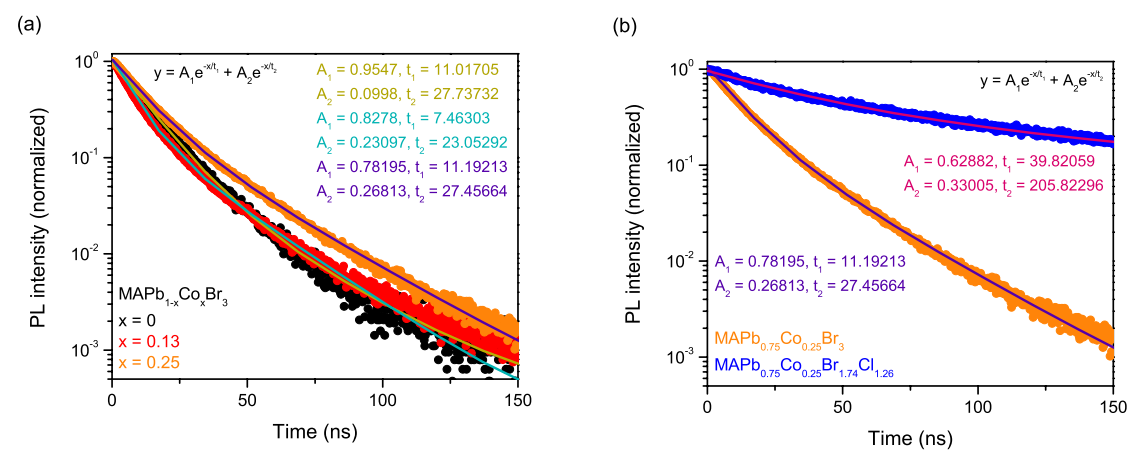
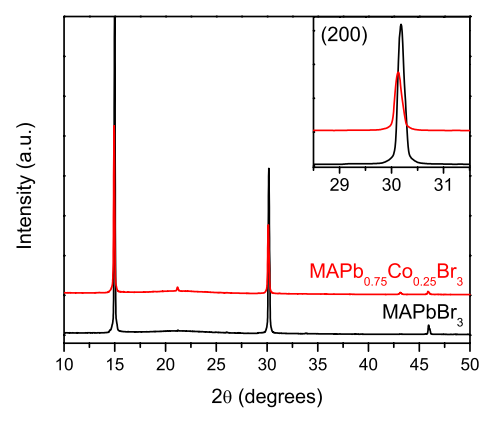


Figure S21. Exponential fits for the time-resolved PL data shown in Figure 4.



**Figure S22.** XRD pattern for MAPbBr<sub>3</sub> (black) and MAPb<sub>0.75</sub>Co<sub>0.25</sub>Br<sub>3</sub> (red) thin films taken with a diffractometer containing a monochromator to filter out Cu  $K\beta$  irradiation. Inset shows zoomed (200) peaks.

**Table S1.** Band gaps extracted from Tauc plots and PL peaks.

MAPb <sub>1-x</sub> Co <sub>x</sub> Br <sub>1-y</sub> Cl <sub>y</sub>	Band Gap (eV)	PL peak (eV)
x = 0, y = 0	2.27	2.30
x = 0.13, y = 0	2.29	2.32
x = 0.25, y = 0	2.31	2.33
x = 0, y = 1.5	2.40	2.52
x = 0.13, y = 1.37	2.37	2.50
x = 0.25, y = 1.25	2.35	2.48

**Table S2.** Lifetimes extracted from exponential fits of time-resolved PL data.

$MAPb_{1-x}Co_{x}Br_{1-y}Cl_{y}$	$\tau_1$ (ns)	$\tau_2$ (ns)	
x = 0, y = 0	11.0	27.7	
x = 0.13, y = 0	7.46	23.1	
x = 0.25, y = 0	11.2	27.5	
x = 0.25, y = 1.25	39.8	206	